RSC Advances

PAPER

Cite this: *RSC Adv.*, 2023, **13**, 1392

Schwann cell-matrix coated PCL-MWCNT multifunctional nanofibrous scaffolds for neural regeneration†

Yas Al-Hadeethi,‡[ab] Aishwarya Nagarajan,‡[c] Srividya Hanuman,[c] Hiba Mohammed,[d] Aakanksha M. Vetekar,[ce] Goutam Thakur,[e] Le N. M. Dinh,[f] Yin Yao,[f] E. M. Mkawi,[a] Mahmoud Ali Hussein,[gh] Vipul Agarwal*[f] and Manasa Nune*[c]

Nerve tissue engineering aims to create scaffolds that promote nerve regeneration in the damaged peripheral nervous system. However, there remain some challenges in the construction of scaffolds in terms of mechanical properties and cellular behaviour. The present work aims to develop multifunctional implantable nanofibrous scaffolds for nerve regeneration. Using electrospinning, nanofibrous neat polycaprolactone (PCL) and PCL/multiwalled carbon nanotubes (PCL-MWCNT) composite scaffolds were prepared in random and aligned morphology. Schwann cells and their secreted biochemical factors are responsible for neuronal survival in the peripheral nervous system. Therefore, the acellular matrix of Schwann cells was spin-coated on the PCL-MWCNT scaffolds to aid nerve regeneration. Physicochemical and mechanical properties, and the *in vitro* cellular response of the developed nanofibrous were investigated. We observed no significant change in fibre diameter between neat PCL and PCL-MWCNT scaffolds regardless of the morphology. However, the inclusion of MWCNT reduced the mechanical strength of nanocomposite scaffolds compared to neat PCL. *In vitro* study revealed biocompatibility of the developed scaffolds both with and without an acellular matrix. Gene expression study revealed a significant increase in peripheral myelin protein (PMP22) expression on acellular matrix-coated PCL-MWCNT scaffolds compared to neat PCL counterparts. Overall, the results suggested Schwann cell matrix-coated PCL-MWCNT nanofibers as a promising conduit for peripheral nerve regeneration.

Received 26th August 2022
Accepted 8th December 2022

DOI: 10.1039/d2ra05368c

rsc.li/rsc-advances

Introduction

Given the complicated physiological system and limited regeneration ability, restoring an injured nervous system remains a challenging task.[1] Current treatment modality in the peripheral nervous system (PNS) involves neurorrhaphy in the case of short nerve injuries and autologous nerve grafts or allografts for larger defects (>10 mm). However, surgical interventions come with considerable risks including size disparities between donor and recipient nerves, neuroma development risks, and infections and disability in complete recovery of function. Lately, nerve tissue engineering has evolved as an alternative strategy to existing clinical modalities.[2] Nerve tissue engineering utilises scaffolds with a range of specific properties including (i) morphology mimicking the extracellular matrix (ECM), (ii) physicochemical and mechanical properties similar to native nerve tissues, and (iii) biodegradability.[3] In addition, in the case of the central nervous system neural scaffold must be electrically conducting to promote regeneration.[4–8]

In PNS, the primary class of glial cells which descend from neural crest cells are called Schwann cells.[9] These support cells play a crucial role in neuronal regeneration. Schwann cells produce ECM components such as laminin, fibronectin, collagen IV, and various proteoglycans necessary for the development and regeneration of neurons. Schwann cells also produce a range of neuropeptides and cell adhesion molecules, both of which are crucial for regulating neuronal survival and

[a]*Department of Physics, Faculty of Science, King Abdulaziz University, Jeddah 21589, Saudi Arabia*
[b]*Lithography in Devices Fabrication and Development Research Group, Deanship of Scientific Research, King Abdulaziz University, Jeddah, 21589, Saudi Arabia*
[c]*Manipal Institute of Regenerative Medicine, Manipal Academy of Higher Education, Manipal 576104, Bengaluru, Karnataka, India. E-mail: manasa.nune@manipal.edu*
[d]*Fondazione Novara Sviluppo, 28100, Novara, Italy*
[e]*Department of Biomedical Engineering, Manipal Institute of Technology, Manipal Academy of Higher Education, Manipal 576104, Karnataka, India*
[f]*Cluster for Advanced Macromolecular Design (CAMD), School of Chemical Engineering, University of New South Wales, Sydney, NSW 2052, Australia. E-mail: agarwalvipul84@gmail.com*
[g]*Department of Chemistry, Faculty of Science, King Abdelaziz University, Jeddah 21589, Saudi Arabia*
[h]*Department of Chemistry, Faculty of Science, Assiut University, Assiut 71516, Egypt*

† Electronic supplementary information (ESI) available. See DOI: https://doi.org/10.1039/d2ra05368c

‡ These authors contributed to the work equally.

axonal growth.[10] Schwann cells also assist in nourishing growing axons by ensheathing and myelinating them. Schwann cells are widely studied for the treatment of demyelinating diseases.[11] In this study, Schwann cells are used to study the regeneration potential of developed scaffolds.

Electrospinning is one of the most widely used scaffold fabrication methods in nerve tissue engineering.[3,12–15] The advantages of using electrospinning include (i) nanofibrous scaffolds mimic ECM, (ii) tuneability of polymer fibre diameter to match native tissue environment, (iii) high porosity allowing exchange of gasses and nutrients, and (iv) tuneability in terms of surface, physicochemical and mechanical properties, and (v) promotes cell adhesion by promoting physical and biochemical cues.[3,16–19] Furthermore, electrospinning allows control over the morphology of scaffolds *i.e.* random *versus* aligned. Surface features (morphology) have been shown to play a crucial role in directing growing axons in neuronal regeneration.[20–22] However, this dependence on surface morphology in providing directional cues for axonal outgrowth is still debated with mixed results reported in the literature. Polycaprolactone (PCL), a biodegradable polymer, has been widely explored in electrospinning for tissue regeneration applications including peripheral nerve regeneration.[12,17,23,24] For example, in one study, surface modified electrospun PCL scaffold was compared against collagen coated electrospun PCL scaffold for peripheral nerve regeneration.[12] In that work, plasma surface modified scaffold exhibited considerably higher (Schwann) cell proliferation and adhesion compared to its collagen coated counterpart. Lee and co-workers explored blended PCL/collagen I electrospun scaffolds in rat peroneal injury model.[23] The implanted scaffold was shown to induce reinnervation and restoration of denervated muscle function 20 weeks after surgery.

Lately, carbon-based fillers have been incorporated in electrospun scaffolds for nerve regeneration primarily to improve the mechanical properties of fabricated scaffolds.[15,25] Recently, PCL was blended with gelatin and graphene to prepare electrospun nanofibrous scaffolds and investigated its efficacy in nerve regeneration using PC12 cells.[24] In that the blended scaffold promoted cell migration, adhesion and proliferation over 7 days. Yu *et al.*[25] fabricated a MWCNT loaded PCL/collagen electrospun scaffold and explored its efficacy in rat sciatic nerve defect model. Compared to a silicon control implant, the MWCNT loaded PCL/collagen electrospun scaffold effectively promoted nerve regeneration and prevented muscle atrophy without invoking body rejection or serious chronic inflammation four months after implantation. Further, MWCNT loaded PCL/collagen electrospun scaffold and silicone conduits performed significantly better than autografted nerve four months after implantation. Recently, Pi *et al.*[26] developed brain-derived neurotrophic factor (BDNF) loaded and polydopamine (PDA) surface modified PCL/MWCNT electrospun scaffolds (PCL/MWCNT/PDA/BDNF) and explored their efficacy in a Schwann cells *in vitro* and in a rat sciatic nerve defect *in vivo* model. *In vitro* studies revealed significant proliferation of Schwann cells cultured on the PCL/MWCNT/PDA/BDNF scaffold along with significant increase in the expression of myelination-related genes (S100, P0, MBP). *In vivo* study revealed similar nerve regeneration response between PCL/MWCNT/PDA/BDNF scaffold and an autograft. They outlined that efficacy of developed scaffold was due to the combination of factors including aligned topography, electrical conductivity of MWCNT, PDA surface modification (polarity) and sustained BDNF release.[26] Taken together from these studies, it is not clear if scaffold morphology along with surface properties can sufficiently promote peripheral nerve regeneration in multicomponent electrospun scaffolds.

In this study, we fabricated PCL and MWCNTs electrospun nanofibrous scaffolds of different morphology (random and aligned) and explored their nerve regeneration potential in Schwann cells. To study the role of surface properties, we coated these scaffolds using an acellular matrix secreted by Schwann cells as an additional surface cue to promote (Schwann) cell growth by providing them with features and biochemical cues naturally experienced by them *in situ*. The biological response of Schwann cells cultured on electrospun scaffolds was evaluated in terms of cell adhesion, proliferation, and gene expression associated with myelination. We observed considerable effect on scaffold morphology and corresponding mechanical properties with the inclusion of MWCNT particularly in aligned scaffolds. However, we did not observe any clear influence of scaffold morphology or surface properties on nerve regeneration potential of Schwann cells.

Experimental

Materials

Polycaprolactone (MW-80 000 g mol^{-1}) in form of pellets was purchased from Sigma-Aldrich (Bengaluru, India). Multiwalled carbon nanotubes (MWCNTs) were purchased in powder form from Sisco Research Laboratories Pvt Ltd (Navi Mumbai, India) diameter of ~30–50 nm and length of 10–30 μm. Methanol, chloroform, dichloromethane, and dimethylformamide were purchased from Himedia Laboratories Pvt Ltd (Mumbai, India). Rat Schwann cell line (RSC96) was procured from ATCC. PBS, DMEM, antibiotic-antimycotic, penicillin and streptomycin were purchased from Gibco (Bengaluru, India).

Preparation of PCL and PCL-MWCNT solution

PCL is soluble in organic solvents such as chloroform and methanol.[27] PCL-MWCNT solution was prepared to contain 10% PCL and 0.005% MWCNT in a 4 : 1 ratio of chloroform to methanol, which was taken on the basis of previous literature[28] and was experimentally optimized here by varying different electrospinning parameters. First, 0.25 mg of MWCNTs was added to 1 ml of methanol which was then ultrasonicated (Ultrasonic cleaner, CD-4831, Codyson, China) for 20 min at room temperature.[29] After ultrasonication, 0.5 g of PCL and 4 ml of chloroform were added, and the solution was stirred overnight.

Electrospinning PCL and PCL-MWCNT nanofibers

To prepare the PCL-MWCNT solution, MWCNT was incorporated with PCL in this project. The electrospinning unit HO-

NFES-040 (Holmarc Opto-Mechatronics Ltd, Kochi, India) has been used to fabricate the scaffolds. Optimization of random fibers was done by varying various parameters like solution concentration, flow rate 6 μl min^{-1}, distance 20 cm, needle gauge size 24 G, and the voltage applied 16 kV.[17,30] Optimization of aligned fibers was done by optimizing the speed of rotation of the mandrel at 2500 rpm and mandrel size 75 mm. The resulting nanofiber mats were kept in a vacuum desiccator for subsequent characterization. The specific scaffolds will be labelled as follows: random PCL (R-PCL), aligned PCL (A-PCL), and MWCNT loaded PCL (PCL-MWCNT).[15]

Physicochemical characterization

Scanning electron microscopy analysis. The surface morphology and diameter of the electrospun nanofibers (PCL, PCL-MWCNT) were determined using a field emission scanning electron microscope (FESEM) equipped with energy dispersive X-ray Spectroscopy (EDX) (FESEM-EDX; JSM 7600F, JEOL, Japan) with a 10 kV accelerating voltage. Prior to imaging, all samples were placed onto SEM stubs and gold sputtering was performed.

Energy dispersive X-ray spectroscopy. Elemental analysis of scaffolds was performed using energy dispersive X-ray analysis at a 15 kV accelerating voltage to detect the presence of CNTs on the surface of the PCL-MWCNT nanofibrous scaffolds.

Mechanical strength analysis. Mechanical properties of the neat PCL and PCL-MWCNT random and aligned nanofibrous scaffolds were evaluated by tensile testing using a Shimadzu universal texture analyzer (EZ-SX) instrument (Shimadzu Corporation, Japan). The electrospun films were trimmed to samples of approximately 40 mm in length and 10 mm in width. Prior to each measurement, the thickness of the sample and the initial distance between two clamps of the instrument, called gauge length, were measured with a digital caliper. The sample was clamped at two ends and subjected to a stretching rate of 20 mm min^{-1} till fracture. The generated measurement results were converted to stress–strain curves using gauge length and cross-sectional area of the films (calculated from the film's width and thickness). Due to the films being light and flexible, some modifications to the stress–strain curves were made. Strain (%) was subtracted by a particular value depending on the films so that the stress–strain slope for Young's modulus calculation starts at the origin. Young's modulus was calculated from the initial elastic region of stress–strain curves. Six films per sample were tested and data is presented as the average ± standard deviation of the six measurements.

Schwann cell culture and extraction of the acellularized matrix (ACM). Rat Schwann cells procured from American Type Culture Collection (ATCC) (CRL-2765 RSC96) were grown in Dulbecco's Modified Eagle Medium supplemented with 10% fetal bovine serum and 1% penicillin-streptomycin and incubated at 37 °C in 5% carbon dioxide. The confluent monolayer of Schwann cells was subjected to serum starvation by replacing the whole media with serum-free DMEM media for 3–5 days. Sterile distilled water was then added to the serum-starved cells and incubated for 1–2 min. After that ammonia solution was added and incubated until the cells detached. The ammonia solution with the cells was discarded and the remaining ECM was scrapped out in PBS using a cell scrapper.[31]

Spin coating and cytochemical characterization of ACM on PCL nanofibrous scaffolds. The extracted ACM was uniformly spread on the scaffolds using the spin coating technique (HO-TH-05, Holmarc Opto-Mechatronics Ltd, Kochi, India).[14] The sterilized scaffolds were first electrospun on the circular coverslips. The coverslip with the scaffold was placed on the spin coating machine and the rotator was spun at 300 rpm for 20 s. 20 μl of ACM solution was added to the center of the spinning coverslip. A thin uniform layer of ACM was coated onto the scaffolds. The ACM-coated scaffolds were further UV sterilized for half an hour for each of the sides before further characterization. Further, cytochemical staining for different components of the extracellular matrix was carried out to qualitatively analyze the coating of Schwann cell-ACM on the scaffolds. To visualize glycoproteins, the ACM was stained using alcian blue and safranin O, and to visualize collagen the scaffolds were treated with Mason's trichome and picrosirius red.[32] ACM coated scaffolds are labelled as: R-PCL + ACM, A-PCL + ACM, R-PCL-MWCNT + ACM, and A-PCL-MWCNT + ACM.

Contact angle analysis. The contact angle of water over the surface of different scaffolds was measured using a goniometer (HO-IAD-CAM-01). The drop of water was manually placed on the top of scaffolds using the sessile drop method. The point where the droplet meets the surface was measured using contact angle image analysis software by Holmarc. Each scaffold was analysed three times and data is presented as average ± standard deviation.

Cell culture studies

Cell seeding on scaffolds. Each side of the electrospun PCL aligned and random nanofibers were sterilized in UV for 2–3 h. In a 24 well plate, ACM-coated and uncoated, random and aligned PCL as well as PCL-MWCNT scaffolds, were placed. Approximately 50 000 cells were seeded on the top of scaffolds for cell adhesion and proliferation studies, while 10 000 cells were seeded for microscopic examinations. Tissue culture polystyrene (TCPS) was used as a control, and the growth medium was changed every other day.[33]

Cell proliferation using MTT assay. MTT analysis is used to quantify cell growth over time on the developed scaffolds. Cell growth was assessed using Schwann cells at 24 and 96 h. After respective time points, culture media was removed, and wells were washed with PBS. Following which MTT reagent and plates were incubated in dark for 3 h at 37 °C as per the manufacturer's protocol. After which, DMSO was added to each well and plate was kept in a shaker for 30–45 min. Following which plate was read using a spectrophotometer (PerkinElmer (Ensight) multimode plate reader (HH34000000)) at 570 nm.

Cell viability assay. The cell viability of cells seeded on scaffolds was evaluated using the standard live/dead test. A live/dead reagent stock solution was made by combining 4 μl of EthD-1 and 1 μl of calcein-AM in 2 ml PBS. Schwann cells were cultured on different scaffolds for 48 h and 96 h. At specific time points, 100–150 μl of live/dead reagent was added to each well,

Table 1 Primer sequences

Primer	Forward sequence	Reverse sequence
GAPDH	GACATGCCGCCTGGAGAAAC	AGCCCAGGATGCCCTTTAGT
PMP22	AATAATCCGCTGCCCGAATCAAG	CTCCGCCTTCAGGGTCAAGTC

and the treated cells were incubated at room temperature for 1 h before imaging. Imaging was conducted using a fluorescence microscope (Nikon Eclipse-TE2000-U).[33]

Immunostaining. Schwann cells were cultured on different scaffolds both with and without ACM treatment. The cells were fixed in 4% paraformaldehyde at 4 °C after 24 h of seeding overnight. The next day cells were permeabilized with 0.3% Triton-X 100 for 15 min, then blocked with 3% BSA for 30–40 min. The cells were incubated with primary antibodies S100β (mouse monoclonal; 1 : 250; Abcam) for 5–6 h. Following the primary antibody, the cells are incubated with a secondary antibody for 1 h with (546 rabbit anti-mouse IgG; 1 : 500; Life-Tech). Following which the secondary antibody was removed, and the scaffolds were stained with DAPI (1 : 1000; HiMedia) for nuclear staining and visualized using a fluorescence microscope (Nikon Eclipse-TE2000-U).[34]

RT-qPCR analysis. Total RNA is extracted from the Schwann cells cultured on the scaffolds for 7 and 14 days using the standard RNA isolation protocol. The obtained RNA is later subjected to cDNA synthesis using the kit from (Biosciences) according to the manufacturer's instruction. Then the mRNA expression is carried out by real-time PCR, using SYBR Green master mix (BioRad). The experiment is carried out in a final volume of 10 μl, containing 0.5 μl of each primer (Table 1), 5 μl of SYBR green master mix, 3.5 μl of diethylpyrocarbonate (DEPC) treated water, and 0.5 μl of cDNA template. The sample was kept in QuantStudio 5 machine for 100 cycles and the result obtained was analyzed using the instrument software.

Statistical analysis. All experiments were carried out in triplicates and the data are presented as average ± standard deviation. p values were determined using Origin software values of $p < 0.05$ was considered statistically significant.

Results and discussion

Surface morphology of electrospun scaffolds

SEM analysis of random and aligned PCL and PCL-MWCNT fibers revealed uniform fibrous morphology (Fig. 1 and S1 (ESI†)). The inclusion of MWCNT caused no noticeable change in the morphology of random nanofibrous scaffolds. However, noticeable change in fibrous morphology was observed in the case of aligned fibres with the inclusion of MWCNT where A-PCL-MWCNT scaffold showing more random morphology compared to A-PCL scaffold (Fig. 1, first row). Fibre diameter analysis revealed the values of 419 ± 150 nm for R-PCL, 330 ± 92 nm for R-PCL-MWCNT, 437 ± 190 nm for A-PCL, and 402 ± 139 nm for A-PCL-MWCNT (n = 100) (Fig. 1a–d). When compared no difference in fiber diameter was observed between random and aligned neat PCL scaffolds (Fig. 1a and c) and random and aligned PCL-MWCNT scaffolds (Fig. 1b and d). Between neat PCL and PCL-MWCNT scaffolds, we noticed some increase in the fiber diameter with the inclusion of MWCNT in the PCL matrix in both random and aligned scaffolds however, the difference did not reach significance. Fiber diameter has been shown to be dependent on filler morphology where fiber diameter increases when using spherical fillers but reduces

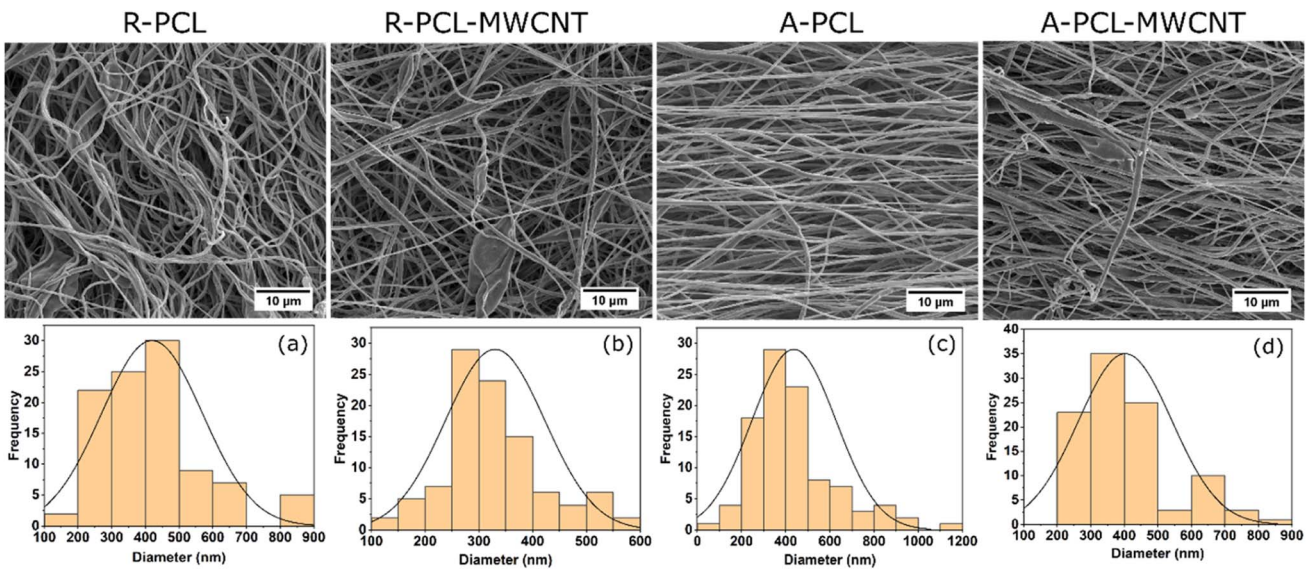

Fig. 1 SEM images of scaffolds (first row) and fibre diameter distribution determined from SEM images by measuring minimum 100 fibres (second row) – (a) R-PCL, (b) R-PCL-MWCNT, (c) A-PCL, (d) A-PCL-MWCNT. Scale bar = 10 μm.

when using tubular or rod-shaped fillers (such as CNT),[15] which is similar to the observed results showing marginal reduction in fiber diameter with the inclusion of MWCNT in the matrix.[34] Nanofibrous scaffolds usually mimic features of ECM as its components have dimensions at the scale of nanometer and micrometer.[35] All the electrospun fibers in this study were in the nanometer range, which is beneficial for cell growth. Aligned fibers are preferred for nerve tissue engineering as it provides contact guidance for the growth of neurons.[44] Fibers that are uniaxially oriented are suitable for aiding the growth of nerves, as it helps the Schwann cells to align along the aligned fibers mimicking the bands of bungner structure which will help in the growth of oriented axons for the regeneration of nerves.[36] Therefore, in this study we compared both random and aligned scaffolds.

Next, we assessed the surface properties of the scaffolds in terms of wettability using water contact angle (values listed in ESI, Table S1†). As anticipated neat PCL scaffolds (R-PCL and A-PCL) exhibited hydrophobic surface properties with contact angle values of ~131° and ~133°, respectively, which are in agreement with previously published reports.[37,38] We observed no considerable change in surface hydrophobicity with the inclusion of MWCNT in both system (random and aligned scaffolds) with values of ~137° (R-PCL-MWCNT) and ~130° (A-PCL-MWCNT). The obtained values were similar to the previous reports on CNT loaded PCL scaffolds.[39] However, surface wettability changed dramatically with ACM coating making the scaffolds more hydrophilic regardless of the matrix morphology and presence of MWCNT (ESI, Table S1†). In the case of random scaffolds, we obtained the values of ~42° and ~54° for R-PCL + ACM and R-PCL-MWCNT + ACM scaffolds, respectively whereas in the case of aligned scaffolds, we obtained values of ~39° and ~50° for A-PCL + ACM and A-PCL-MWCNT + ACM scaffolds, respectively. Such significant reduction in contact angle due to ACM coating can be attributed to the composition of ACM comprising hydrophilic compounds including proteins, proteoglycans and glycosaminoglycans. Further, the increase in contact angle in ACM coated MWCNT containing scaffolds compared to their neat polymer counterparts (R-PCL + ACM and A-PCL + ACM) can be attributed to the hydrophobic nature of MWCNT.

Mechanical strength

The mechanical properties of neat PCL and MWCNT loaded PCL scaffolds were explored by using tensile testing. The obtained stress strain curves and mechanical properties of the scaffolds are presented in Fig. 2 (and ESI Table S2†). We observed a significant reduction in tensile strength with the inclusion of MWCNT in the aligned scaffolds (A-PCL) matrix (A-PCL-MWCNT: 5.20 ± 2.40 MPa compared to A-PCL: 15.73 ± 5.74 MPa). Contrarily, no change in tensile strength was observed in the case of random scaffolds with the inclusion of MWCNT (R-PCL-MWCNT: 6.10 ± 1.70 MPa compared to R-PCL: 3.31 ± 1.75 MPa). Tensile strength reflects the highest stress tolerated by a scaffold before failure. Taken together, it was inferred that aligned neat PCL scaffold (A-PCL) exhibited highest tensile strength which could be due to the specific aligned morphology of fibres in line with previous observations. Scaffolds with aligned fibres dissipate stress more efficiently than random fibres which could explain the significantly superior tensile strength of A-PCL compared to other scaffolds. The significant reduction in the tensile strength in A-PCL-MWCNT compared to A-PCL could be due to the interference of MWCNT during electrospinning leading to considerable change in scaffold morphology (relatively random morphology instead of neatly aligned fibres). This inference is further supported by similar tensile strength values between random scaffolds [R-PCL (3.31 ± 1.75 MPa) and R-PCL-MWCNT (6.10 ± 1.70 MPa)] and A-PCL-MWCNT (5.20 ± 2.40 MPa).

Similar to tensile strength, we observed no noticeable difference in elongation at break between R-PCL-MWCNT (145.37 ± 33.62%) compared to R-PCL (131.05 ± 21.66%) indicating that MWCNT caused no change in the behaviour of electrospun PCL scaffolds in random morphology. However, elongation at break increased from 46.74 ± 3.38% (A-PCL) to 72.44 ± 13.39% (A-PCL-MWCNT) in the case of aligned scaffolds with the inclusion of MWCNTs. This marginal improvement in elongation at break could be attributed to the change in morphology of the scaffolds leading to (i) presumably combinatorial effect of PCL fibres and MWCNTs – resulting in relatively flexible scaffold, and (ii) MWCNT did not interact with PCL fibers to form entangled structures needed to dissipate

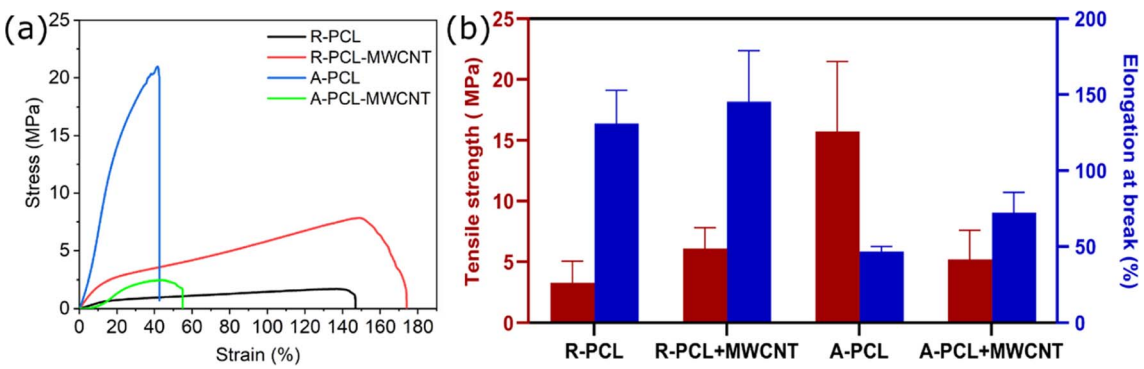

Fig. 2 Mechanical properties of neat PCL and PCL-MWCNT scaffolds – (a) representative stress–strain curves, and (b) tensile strength and elongation at work. Data are presented as average ± standard deviation ($n = 3$).

stress throughout the matrix. Taken together it was deduced that random scaffolds (R-PCL and R-PCL-MWCNT) exhibited significantly higher elongation at break compared to aligned scaffolds (A-PCL and A-PCL-MWCNT) (Fig. 2b). A reduction in mechanical properties (tensile strength) with the inclusion of carbon fillers has been previously reported for polymer/carbon filler-based nanocomposites including CNT, graphene oxide, and graphene.[40]

Cytochemical characterization of ACM

Cytochemical characterization of Schwann cells and Schwann cell-derived acellularized matrix (ACM) to detect components of extracellular matrix (ECM). The presence of collagen, proteoglycans, and glycoproteins was detected using stains such as alcian blue, Masson's trichome, picrosirius red and safranin O (Fig. 3). The blue color of alcian blue is because of the presence of Cu in molecules and also has a solution of 3% of acetic acid and it can stain carboxylated mucopolysaccharides and sulfated and glycoproteins (sialomucins) by forming salt linkages with acid groups of acid mucopolysaccharides. The stain molecule carries a positive charge and gets attracted to the negative mucins. In the picrosirius red stain, the sulphonic acid group in Sirius red reacts with collagen molecules by reacting with amino groups lysine and hydroxylysine and guanidine groups of arginine, thereby being an anionic dye, it attaches to different isoforms of collagen. Masson's trichrome has 3 dyes that stain fibrin, erythrocytes, and collagen fibers. Acidic dye initially stains cells that bind with phosphoacids, less permeable components retain the red color whereas collagen binds to aniline blue. Safranin O is a cationic stain, stains sulfated glycosaminoglycans forming a reddish-orange complex, but binding makes it appear red. It was observed that the Schwann cell ACM has retained all the ECM constituents indicated by the positive staining which is comparable to the cellular control.

Further, the Schwann cell ACM was coated and stained on the scaffolds: R-PCL and R-PCL-MWCNT to observe how well the ECM constituents were retained after coating on them (Fig. S2†). Uncoated R-PCL was used as a control. We did not perform this experiment on the aligned scaffolds as there would be no difference with the fiber orientation. There was certain amount of staining observed on the uncoated control as well which is because of the porous nanofibrous scaffolds absorbing the dyes. This is also ascertained by the color differences detected between the ACM coated on the culture dishes (Fig. 3) *vs.* scaffolds. Nevertheless, there was clear difference in the staining intensities visualized between the coated and uncoated samples. We could also see thick patchy fibrous deposits on the ACM coated samples demonstrating the ACM presence, while the uncoated scaffold had clear and uniform appearance. However, there was no intensity difference seen between the PCL-MWCNT and PCL scaffolds.

Cell proliferation

MTT assay was conducted to determine the proliferation of Schwann cells on different scaffolds. From the graph in Fig. 4, we observed a gradual increase in the cell proliferation in all the scaffolds over 96 h, however, the values did not reach significance. We observed a relatively higher cell proliferation at both 24 and 96 h in random scaffolds (with and without MWCNT and ACM) compared to their aligned counterparts. The observed results are in agreement with previous report by Gnavi *et al.*[41] showing that gelatin aligned nanofibers had shown lesser proliferation rates compared to the random fibers in both primary Schwann cells as well as RT4-D6P2T cells which was

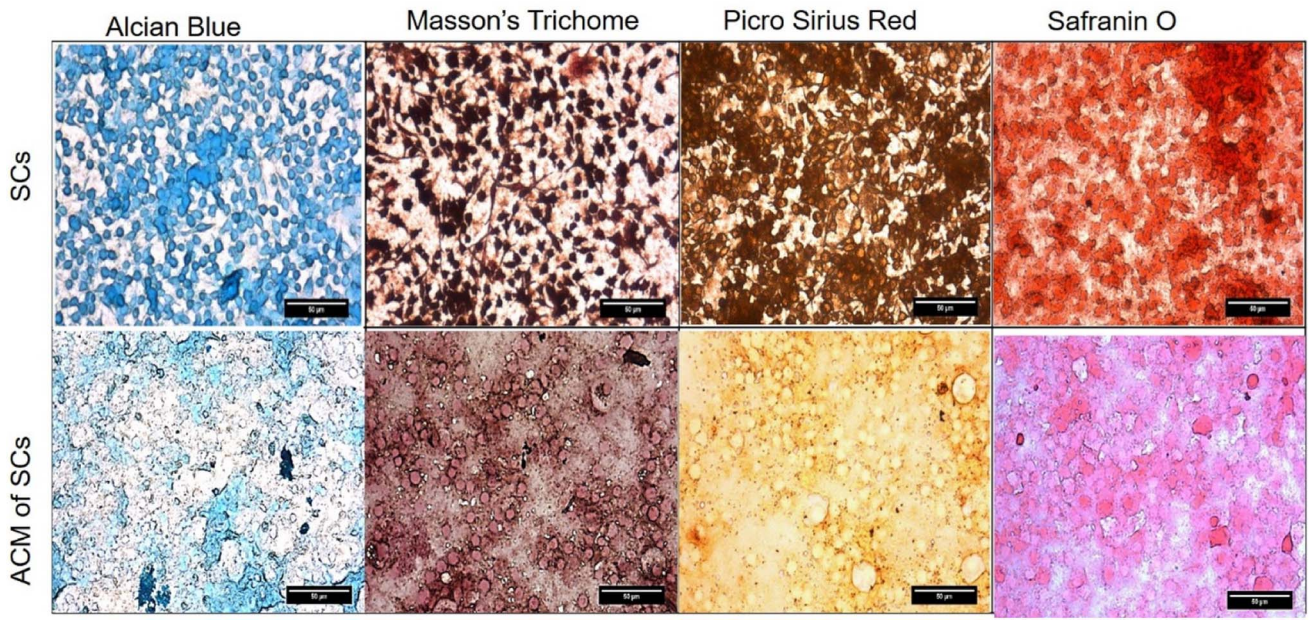

Fig. 3 Cytochemical characterization of Schwann cells and Schwann cell-ACM were stained with alcian blue, Masson's trichome, Picro Sirius red and Safranin O.

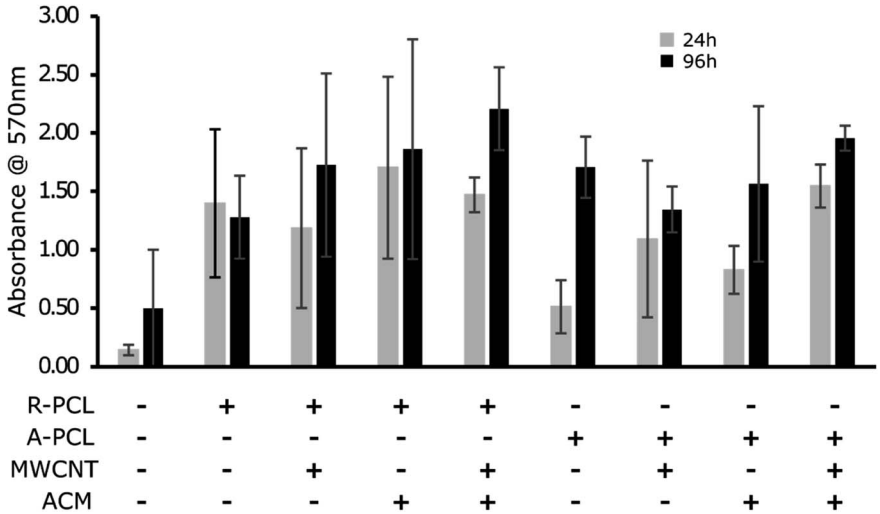

Fig. 4 Cell proliferation assay showing cell growth over the period of 24 h and 96 h post incubation with the different scaffolds (random and aligned) with and without MWCNT and ACM coating. Data presented as average ± standard deviation ($n = 4$). The considerable variance can be attributed to the interaction of dye with electrospun PCL fibres.

attributed to the lesser focal adhesion points and different scaffolds topography on the aligned scaffolds compared to the random scaffolds. We also observed a noticeable difference between control TCPS and electrospun scaffolds regardless of scaffold morphology. The electrospun scaffolds exhibited considerably higher cell proliferation at both 24 and 96 h than TCPS control. Further marginal increase in cell proliferation in ACM coated scaffolds (R-PCL + ACM, R-PCL-MWCNT + ACM, A-PCL-MWCNT + ACM) compared to their uncoated counterparts expect for A-PCL. This increase in cell proliferation can be attributed to the combination of factors including (i) hydrophilicity of surface (as observed in contact angle analysis), and (ii) presence of innate matrix comprising proteins, proteoglycans and glycosaminoglycans (found in ACM) which could promote cell adhesion and simultaneously provide feedback mechanism to induce cell growth. These observations are in line with previous works highlighting the importance of surface topography and polarity on cell behaviour including proliferation, adhesion and differentiation.[12,21,25,26,42] However, again the change did not reach significance. Taken together, fabricated scaffolds exhibited high biocompatibility with prominent cell proliferation over time. These results are in agreement with previous studies which showed that the addition of CNTs did not change the viability percentage of astrocytes on PCL fibers,[39] BMSCs on PCL/gelatin/CNT random and aligned nanofibers,[41] and proliferation rate of rabbit Schwann cells on poly(*p*-dioxanone) nanofiber yarns.[8] Thus, indicating that CNTs were biocompatible with no cellular toxicity.[39]

Cell viability study

Cell viability was studied using the standard live/dead assay at two different time intervals (48 and 96 h). Schwann cells cultured on different scaffolds were stained using calcein AM/ethidium bromide I stain resulting in live cells fluorescing green while dead cells fluorescing red.[43,44] Fluorescence images in Fig. 5 revealed an almost negligible number of dead (red) cells at 48 h regardless of the scaffold highlighting the biocompatibility of the developed scaffolds. At 96 h, we observed the presence of some dead cells in different scaffolds, however, the numbers were marginal compared to live (green) cells in culture (regardless of the scaffold). It was concluded that both treated (ACM coated)- and untreated (uncoated)-scaffolds regardless of the presence of MWCNT maintained Schwann cells viability over 96 h.

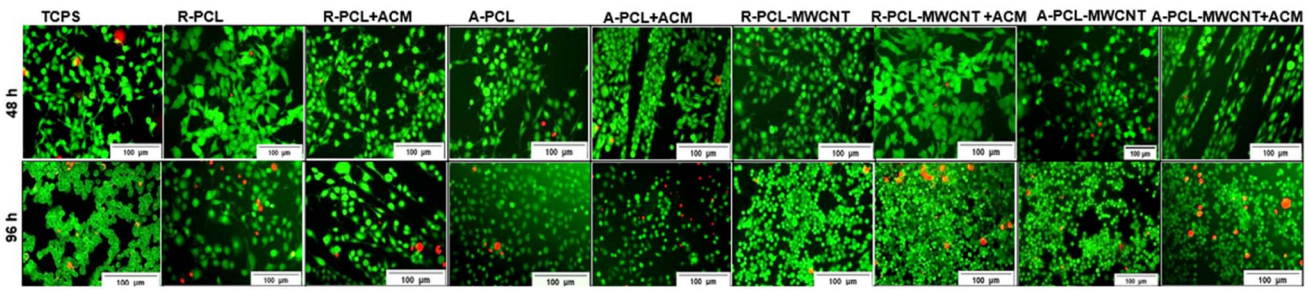

Fig. 5 Live-dead cell viability assay showing live (green) and dead (red) Schwann cells cultured over the period of 48 and 96 h on different scaffolds (random and aligned) with and without MWCNT and ACM coating. Scale bar: 100 μm.

The addition of MWCNTs to the PCL/gelatin scaffold has been previously shown to aid Schwann cell maturation.[45] Similar results were observed in this work where an increase in cell growth was observed at 96 h compared to 48 h which indicates that fabricated scaffolds promote cell viability over time. Also, in our previous work, we observed that there was a prominent increase in the ACM-coated scaffolds showing the positive effect of the Schwann cells ECM on promoting cellular proliferation and retaining their bipolar extended morphology.[46] Thus, it was envisaged that ACM coated aligned scaffolds (with and without MWCNT) would give an added advantage in bringing in the multifunctional nature of the scaffolds which is an ideal biomaterial property for nerve tissue engineering applications.

Immunostaining

Immunostaining with S100β which is a predominant marker expressed in most stages of Schwann cell maturation shows that it is expressed on all types of scaffolds. All of its functions involve interaction with a wide range of target proteins which control proliferation, differentiation, apoptosis, Ca^{2+} homeostasis, energy metabolism, and inflammation.[47] S100β is a phenotypic marker of Schwann cells which is expressed in their cytoplasm. We stained cells cultured on different scaffolds with S100β antibody to elucidate any change in the Schwan cell phenotype. As shown in Fig. 6, we observed typical bipolar extension of Schwann cells prominently on the ACM-treated scaffolds compared to the untreated scaffolds. This study shows that ACM-treated samples offer more hydrophilic conditions for Schwann cells to adhere to and support the maintenance of their physiological phenotype in line with previously published reports.[53] This indicates that the inclusion of MWCNTs, as well as ACM, was advantageous for the phenotypic maintenance of Schwann cells when cultured on developed scaffolds. Similar results were observed by Wu *et al.*[48] In their study, composite nanofiber yarns based on poly(*p*-dioxanone) (PPDO) and CNTs were used where rabbit Schwann cells cultured on them also did not show any significant difference in the expression of the S100β.

Gene expression

Myelination is one of the important prerequisites for complete functional nerve recovery. Peripheral myelin protein 22 (PMP22) is a promyelinating factor expressed by Schwann cells and regulates the growth of myelinating Schwann cells.[49] From gene expression studies (Fig. 7), it is evident that there is a significant change in PMP22 expression in ACM-treated scaffolds compared to their untreated counterparts at both 7 and 14 d. This significance is more prominently observed in the R-PCL-MWCNT scaffolds with and without the ACM coating. However, there was no change observed in PMP22 expression in aligned scaffolds. These results are in congruence with a previous study by Chew *et al.*,[50] where human Schwann cells were cultured on PCL aligned and random fibers. In that study, they observed no significant difference in the expression of pro-myelinating genes such as PMP22, myelin basic protein (MBP), and myelin-associated glycoprotein (MAG) between random and aligned scaffolds.[50] In our study, we also observed that the Schwann cells ACM treatment has significantly advanced the PMP22 expression in the expected manner due to the inherent nature of Schwann cells aiding in myelination. Also, MWCNT addition has shown similar results irrespective of the ACM treatment.[48] This is in agreement with studies where MWCNT addition to PCL/gelatin nanofibers and PPDO nanofiber yarns promoted the expression of other myelin proteins such as myelin protein zero (MPZ/P0) and MBP.[51] Interestingly, we observed that the combination of MWCNTs with ACM further enhanced PMP22 expression in a significant way. This could be because the MWCNTs interact with the proteins present in the ACM in a better way as they resemble the three-dimensional arrangement of the natural ECM in the form of collagen nanotubes. MWCNTs can allow a simulation of *in vivo* conditions *in vitro* to induce natural cellular processes, such as cellular differentiation. This provides the stable attachment of cells to the scaffold surface and begins the differentiation processes such as myelination.[52] Thus, the combination of MWCNTs with Schwann cells ACM promoted cell-specific functions such as myelination proving it to be an ideal biomaterial for peripheral nerve regeneration applications.

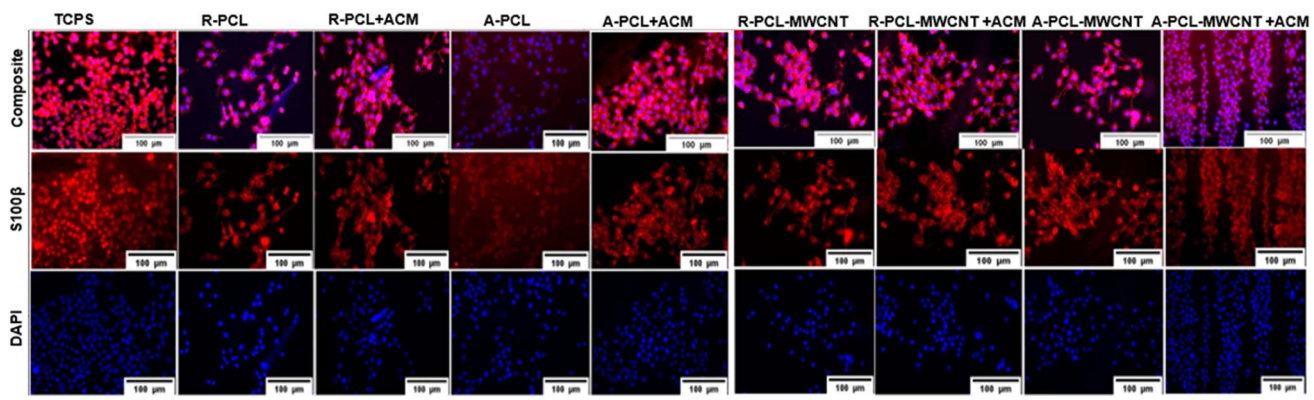

Fig. 6 Immunostaining of Schwann cells cultured on different scaffolds using a S100β antibody. DAPI (blue) stains the nuclei and the antibody S100β (red) stains the Schwann cell structure. TCPS represents untreated control.

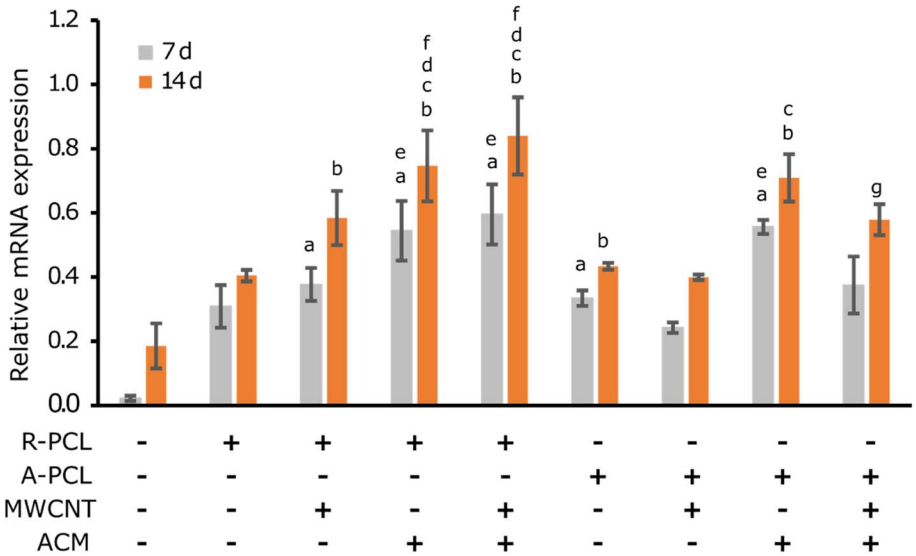

Fig. 7 RT-PCR analysis of PMP22 gene expression of Schwann cells cultured on various nanofibrous scaffolds with or without ACM at two-day points: day 7 and day 14. Results are represented as mean ± standard deviation ($n = 2$). One-way ANOVA with Bonferroni test for multiple comparisons was used for statistical analyses for all quantification studies where a, b, c, d, e, f and g represent significant difference ($p < 0.05$) over TCPS 7 d, TCPS 14 d, R-PCL 14 d, A-PCL 14 d, A-PCL-MWCNT 7 d, A-PCL-MWCNT 14 d, and A-PCL + ACM 14 d, respectively.

Conclusions

In the current work, we aimed to decipher the impact of surface properties and scaffold morphology on nerve regeneration. To this end, we fabricated PCL and MWCNTs electrospun nanofibrous scaffolds of different morphology (random and aligned) coated them with acellular matrix secreted by Schwann cells. SEM images revealed change in surface morphology of aligned fibres with the inclusion of MWCNT. However, inclusion of MWCNT caused no change in fibre diameter and surface hydrophobicity (contact angle) amongst neat PCL and PCL-MWCNT scaffolds regardless of morphology. *In vitro* studies confirmed the biocompatibility of scaffolds with no noticeable effect of ACM coating or presence of MWCNT observed. We observed significant difference in ACM coated scaffolds in terms of PMP22 gene expression compared to their uncoated counterparts regardless of morphology. This study indicates that surface properties of electrospun scaffolds may play a relatively more influential role than scaffold morphology in nerve regeneration.

Author contributions

Conceptualization, M. N., methodology, M. N., Y. A., A. N., A. V., S.·H., L. N. M. D., V. A.; software, A. N., S.·H., Y. A., H. M., M. M., M. H., V. A.; writing original draft preparation, M. N., G. T., A. N., S.·H., V. A.; writing review and editing, Y. A., M. N., G. T., V. A.; visualization, M. N.; supervision, Y. A., M. N. and V. A.; funding acquisition, Y. A. All authors have read and agreed to the published version of the manuscript.

Conflicts of interest

There are no conflicts to declare.

Acknowledgements

The Deanship of Scientific Research (DSR) at King Abdulaziz University (KAU), Jeddah, Saudi Arabia has funded this project, under grant no. (KEP-PhD: 72-130-1443).

References

1 R. Boni, A. Ali, A. Shavandi and A. N. Clarkson, *J. Biomed. Sci.*, 2018, **25**, 90.
2 J. Ai, A. Kiasat-Dolatabadi, S. Ebrahimi, A. Ai, N. Lotfibakhshaiesh, A. Norouzi Javidan, H. Saberi, B. Arjmand and H. Aghayan, *Arch. Neurosci.*, 2013, **1**, 15–20.
3 A. Saudi, S. M. Zebarjad, H. Alipour, E. Katoueizadeh, A. Alizadeh and M. Rafienia, *Mater. Chem. Phys.*, 2022, **282**, 125868.
4 P. Sensharma, G. Madhumathi, R. D. Jayant and A. K. Jaiswal, *Mater. Sci. Eng., C*, 2017, **77**, 1302–1315.
5 X. Gu, F. Ding and D. F. Williams, *Biomaterials*, 2014, **35**, 6143–6156.
6 N. Zhang, H. Liumin and W. Wu, *Neural Regener. Res.*, 2016, **11**, 717.
7 Z. X. Meng, W. Zheng, L. Li and Y. F. Zheng, *Mater. Sci. Eng., C*, 2010, **30**, 1014–1021.
8 M. Nune, A. Subramanian, U. M. Krishnan and S. Sethuraman, *J. Tissue Eng. Regener. Med.*, 2019, 2860.
9 K. Bhatheja and J. Field, *Int. J. Biochem. Cell Biol.*, 2006, **38**, 1995–1999.
10 L. Ning, H. Sun, T. Lelong, R. Guilloteau, N. Zhu, D. J. Schreyer and X. Chen, *Biofabrication*, 2018, **10**, 035014.
11 A. Hopf, D. J. Schaefer, D. F. Kalbermatten, R. Guzman and S. Madduri, *Cells*, 2020, **9**, 1990.

12 M. P. Prabhakaran, J. Venugopal, C. K. Chan and S. Ramakrishna, *Nanotechnology*, 2008, **19**, 455102.
13 N. Ghane, S. Khalili, S. Nouri Khorasani, R. Esmaeely Neisiany, O. Das and S. Ramakrishna, *J. Biomed. Mater. Res., Part A*, 2021, **109**, 437–452.
14 X. Xie, Y. Chen, X. Wang, X. Xu, Y. Shen, A. Aldalbahi, A. E. Fetz, G. L. Bowlin, M. El-Newehy and X. Mo, *J. Mater. Sci. Technol.*, 2020, **59**, 243–261.
15 R. Scaffaro, M. Gammino and A. Maio, *Compos. Sci. Technol.*, 2022, **221**, 109363.
16 V. Agarwal, D. Ho, D. Ho, Y. Galabura, F. Yasin, P. Gong, W. Ye, R. Singh, A. Munshi and M. Saunders, *ACS Appl. Mater. Interfaces*, 2016, **8**, 4934–4939.
17 S. R. K. Meka, S. Kumar Verma, V. Agarwal and K. Chatterjee, *ChemistrySelect*, 2018, **3**, 3762–3773.
18 K. D. McKeon-Fischer, D. P. Browe, R. M. Olabisi and J. W. Freeman, *J. Biomed. Mater. Res., Part A*, 2015, **103**, 3633–3641.
19 A. Maio, M. Gammino, E. F. Gulino, B. Megna, P. Fara and R. Scaffaro, *ACS Appl. Polym. Mater.*, 2020, **2**, 4993–5005.
20 B. Li, V. Agarwal, D. Ho, J.-P. Vede and K. S. Iyer, *New J. Chem.*, 2018, **42**, 7237–7240.
21 D. Ho, J. Zou, X. Chen, A. Munshi, N. M. Smith, V. Agarwal, S. I. Hodgetts, G. W. Plant, A. J. Bakker and A. R. Harvey, *ACS Nano*, 2015, **9**, 1767–1774.
22 W. Zhu, C. O'Brien, J. R. O'Brien and L. G. Zhang, *Nanomedicine*, 2014, **9**, 859–875.
23 B.-K. Lee, Y. M. Ju, J.-G. Cho, J. D. Jackson, S. J. Lee, A. Atala and J. J. Yoo, *Biomaterials*, 2012, **33**, 9027–9036.
24 M. Heidari, S. H. Bahrami, M. Ranjbar-Mohammadi and P. Milan, *Mater. Sci. Eng., C*, 2019, **103**, 109768.
25 W. Yu, X. Jiang, M. Cai, W. Zhao, D. Ye, Y. Zhou, C. Zhu, X. Zhang, X. Lu and Z. Zhang, *Nanotechnology*, 2014, **25**, 165102.
26 W. Pi, Y. Zhang, L. Li, C. Li, M. Zhang, W. Zhang, Q. Cai and P. Zhang, *Biofabrication*, 2022, **14**, 035006.
27 M. Nune, P. Kumaraswamy, U. Maheswari Krishnan and S. Sethuraman, *Curr. Protein Pept. Sci.*, 2013, **14**, 70–84.
28 B. Azimi, P. Nourpanah, M. Rabiee and S. Arbab, *J. Eng. Fibers Fabr.*, 2014, **9**, 155892501400900320.
29 S. Hanuman and M. Nune, *Regener. Eng. Transl. Med.*, 2022, **8**, 334–344.
30 S. K. Sharma, *Handbook of Materials Characterization*, Springer, 2018.
31 M. Sivan, D. Madheswaran, M. Asadian, P. Cools, M. Thukkaram, P. Van Der Voort, R. Morent, N. De Geyter and D. Lukas, *Surf. Coat. Technol.*, 2020, **399**, 126203.
32 L. N. M. Dinh, B. N. Tran, V. Agarwal and P. B. Zetterlund, *ACS Appl. Polym. Mater.*, 2022, **4**, 1867–1877.
33 M. L. P. Ha, B. P. Grady, G. Lolli, D. E. Resasco and W. T. Ford, *Macromol. Chem. Phys.*, 2007, **208**, 446–456.
34 V. Agarwal, F. M. Wood, M. Fear and K. S. Iyer, *Aust. J. Chem.*, 2017, **70**, 280.
35 A. Hu, B. Zuo, F. Zhang, Q. Lan and H. Zhang, *Neural Regener. Res.*, 2012, **7**, 1171–1178.
36 M. Suryamathi, C. Ruba, P. Viswanathamurthi, V. Balasubramanian and P. Perumal, *Macromol. Res.*, 2019, **27**, 55–60.
37 S. R. K. Meka, V. Agarwal and K. Chatterjee, *Mater. Sci. Eng., C*, 2019, **94**, 565–579.
38 R. Ghobeira, M. Asadian, C. Vercruysse, H. Declercq, N. De Geyter and R. Morent, *Polymer*, 2018, **157**, 19–31.
39 M. Srikanth, R. Asmatulu, K. Cluff and L. Yao, *ACS Omega*, 2019, **4**, 5044–5051.
40 M. Nune, U. M. Krishnan and S. Sethuraman, *RSC Adv.*, 2015, **5**, 88748–88757.
41 S. Gnavi, B. E. Fornasari, C. Tonda-Turo, R. Laurano, M. Zanetti, G. Ciardelli and S. Geuna, *Int. J. Mol. Sci.*, 2015, **16**, 12925–12942.
42 K. SwaminathanáIyer, *New J. Chem.*, 2018, **42**, 7237–7240.
43 S. W. Crowder, Y. Liang, R. Rath, A. M. Park, S. Maltais, P. N. Pintauro, W. Hofmeister, C. C. Lim, X. Wang and H.-J. Sung, *Nanomedicine*, 2013, **8**, 1763–1776.
44 M. Nune, A. Subramanian, U. M. Krishnan, S. S. Kaimal and S. Sethuraman, *Nanomedicine*, 2017, **12**, 219–235.
45 M. Mohammadi, A. Ramazani SaadatAbadi, S. Mashayekhan and R. Sanaei, *J. Appl. Polym. Sci.*, 2020, **137**, 49219.
46 M. Nune, M. Bhat and A. Nagarajan, *J. Med. Biol. Eng.*, 2022, **42**, 147–156.
47 S. Y. Chew, Y. Wen, Y. Dzenis and K. W. Leong, *Curr. Pharm. Des.*, 2006, **12**, 4751–4770.
48 S. Wu, Y. Qi, W. Shi, M. Kuss, S. Chen and B. Duan, *Acta Biomater.*, 2022, **139**, 91–104.
49 L. Pan, X. Pei, R. He, Q. Wan and J. Wang, *Colloids Surf., B*, 2012, **93**, 226–234.
50 C. Z. Chen, B. Neumann, S. Förster and R. J. M. Franklin, *Open Biol.*, 2021, **11**, 200352.
51 F. M. Tonelli, A. K. Santos, K. N. Gomes, E. Lorençon, S. Guatimosim, L. O. Ladeira and R. R. Resende, *Int. J. Nanomed.*, 2012, **7**, 4511.
52 Y.-S. Chen and G.-H. Hsiue, *Biomaterials*, 2013, **34**, 4936–4944.
53 L. Pan, X. Pei, R. He, Q. Wan and J. Wang, *Colloids Surf., B*, 2012, **93**, 226–234.